Optimization of Flywheel Rotor Energy Density and Stability

Daniel Coppede , Fabio da Silva Bortoli , Joao Manoel Losada Moreira , Nadja Simao Magalhaes , Carlos Frajuca *

Posted Date: 12 December 2023

doi: 10.20944/preprints202312.0530.v1

Keywords: flywheel; flywheel rotor; flywheel stability; flywheel energy density

Article

Optimization of Flywheel Rotor Energy Density and Stability

Daniel Coppede [1], Fabio da Silva Bortoli [2], Joao Manoel Lozada Moreira [1], Nadja Simao Magalhaes [3] and Carlos Frajuca [2,4,*]

[1] Universidade Federal do ABC; joao.moreira@ufabc.edu.br, www.ufabc.edu.br
[2] Instituto Federal de Sao Paulo; frajuca@ifsp.edu.br, www.ifsp.edu.br
[3] Universidade Federal de Sao Paulo; nadja.magalhaes@unifesp.br, https://www.unifesp.br/campus/dia/#
[4] Universidade Federal de Rio Grande; frajuca@furg.br, www.furg.br
* Correspondence: frajuca@gmail.com; Tel.: 5511987229644

Abstract: A study on flywheel geometries is presented based on finite element modelling simulations. The study analyses the stress behaviour of flywheel rotors subjected to the rotational speed that creates the maximum stress that the flywheel can support, and then calculates the rotational-energy-to-mass ratio (energy density) for each geometry. The geometry that presented the best performance was the one with a Gaussian section for the flywheel rotor. The material used in the simulations was carbon fibre Hexcel UHM 12000. The best results using a single disk were under a rotational speed of ≈279000 rpm and a rotational energy density of ≈ 440 Wh/kg. However, these values still yielded low total energy. To increase the total energy, flywheels with 2 and 3 rotors were analysed, particularly in regard to stability. As some instability was found, a solution was developed.

Keywords: flywheel; flywheel rotor; flywheel stability; flywheel energy density

1. Introduction

A flywheel is a rotational device that stores rotational energy as it spins. When this energy can be converted into electrical energy, it is called an electromechanical battery [1–3] which, in the simplest way, is referred to as the first generation. The second generation incorporates an AC generator, an inverter and a rectifier. If it reaches the power grid and the flow of energy can be reversed, it becomes a Flywheel Energy Storage System (FESS) [2,3]. The third generation [3–6] includes more characteristics (magnetic bearings, vacuum, etc). New and expensive materials can improve the range of energy storage, but as they are expensive it is desirable to increase the stored energy density through new geometries.

Figure 1 shows the evolution of the flywheel generations [2–4]. It also shows that the important goal at the present is to reach a very high energy density storage. As can be seen in the figure, the energy density depends on the material that is used to fabricate the flywheel. For instance if the flywheel could be made of carbon nanotubes (CNT) it could reach an energy density that is about 20% of gasoline's energy density, if an efficiency of 20% is considered for a combustion engine and an efficiency of 99% is considered for flywheels; therefore, their performances could be quite close.In this case, such flywheels could perhaps replace gasoline tanks as energy storage devices. They could even be used in aeroplanes.

Other electrical properties of Flywheels are very important but let's consider that they are advanced enough at present to fulfil the requirements.

To reach such a goal many simulations using finite elements method (FEM) with a variety of geometries were made using the von Mises criterion to determine the maximum allowed stress on the Flywheel, followed by simulations of the normal vibration modes to verify the rotational stability of the system.

The rotational energy density in a flywheel is estimated by the formula [7–9]:

Preprints (www.preprints.org) | NOT PEER-REVIEWED | Posted: 12 December 2023 doi:10.20944/preprints202312.0530.v1

$$\frac{E}{M} = \frac{\sigma_{max}}{2\rho}, \quad (1)$$

where E is the rotational energy stored, m is the mass of the rotating flywheel, σ_{max} is the material's ultimate tensile stress and ρ is the material's specific mass. Using equation (1), in Table 1 examples are shown of energy densities for different materials [8,10]. The material used in the simulations of this work appears in the last line of Table 1: Carbon-Fiber-Hexcel-UHM-12000.

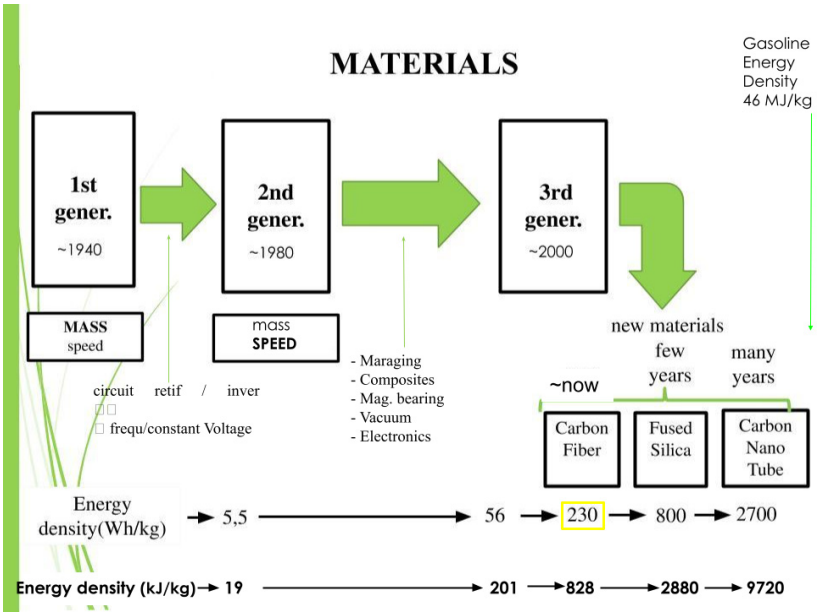

Figure 1. The figure presents the evolution of flywheels with emphasis in the fabrication material. Flywheels made of Carton NanoTubes (CNT) are expected to store energy at the rate of one fifth of gasoline's storage; however, taking into account the efficiency, the former might equalise with the latter. Source: The authors.

Table 1. Materials used in the fabrication of flywheels. Data from [8], except Hexcel UHM Carbon Fibre 12000 (source MatWeb [10]). Results shown in the last column were calculated from eqn. (1).

Material	Ultimate tensile Stress (MPa)	Specific mass (kg/m³)	Flywheel energy density (Wh/kg)
7075 Aluminium	572	2810	28
17-7 PH Stainless steel	1650	7800	29
Ti-15V-3Cr-3Al-3Sn ST 790 °C	1380	4760	40
E-glass (glass-fibre) laminated	~1400	2146	90
T1000G laminated (Toray)	3040	1800	234
T1000G fibre only (Toray)	6370	1800	491
Carbon-Nano-Fibres	2920	2000	202
Carbon-Fiber-Hexcel-UHM-12000	3730	1870	277

Coppede [11] performed simulations using a finite-element analysis of flywheels made of two materials: Maraging steel (AISI 18 Ni 350) and carbon fibre (Hexcel UHM 12000), with carbon fibre as a reinforcement. His main result indicates that the best option is to make the flywheel only with carbon fibre, as can be seen in Figure 2.

This work presents a series of simulations with the intention to optimise the rotational energy density that can be stored in a flywheel, also analysing the stability of the system under high rotational speeds. The second section describes materials and methods used during the simulations. In the third section the results for maximum rotational speed and the von Mises stress distribution are presented. Later in the same section the simulations about stability using vibrational modes are

Preprints (www.preprints.org) | NOT PEER-REVIEWED | Posted: 12 December 2023 doi:10.20944/preprints202312.0530.v1

presented and some solution for a stability problem is presented. The fourth section presents a discussion about the results.

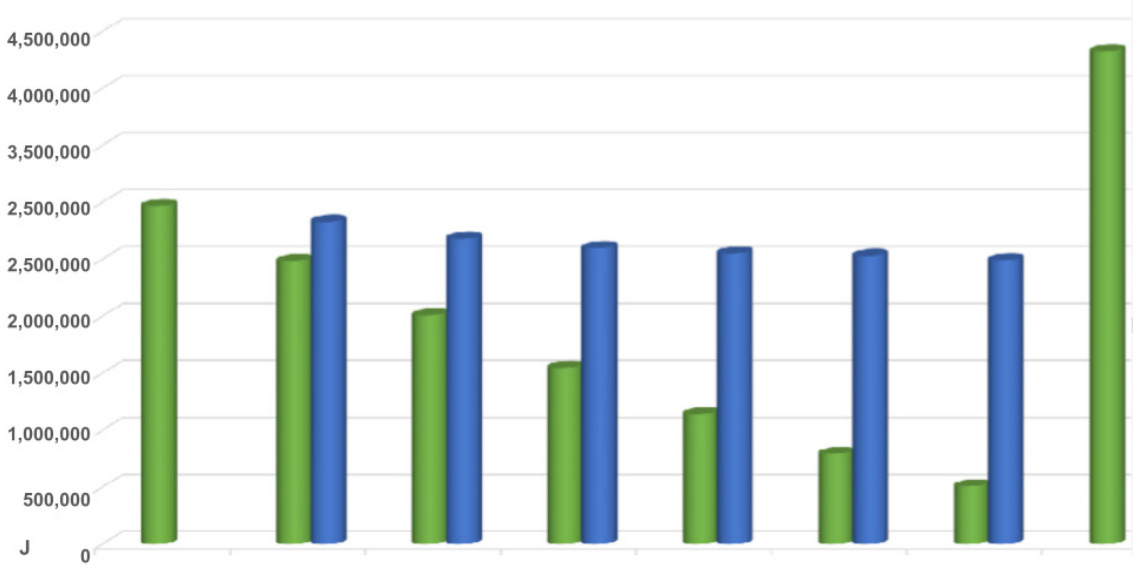

Figure 2. Several FEM simulations were performed using flywheels made of Maraging steel, carbon fibre and Maraging steel revested with carbon fibre. The figure shows the total rotational energy (in J): in green is the rotational energy in the Maraging steel and in blue is the rotational energy in the carbon fibre. From the left to right: pure Maraging steel, then the carbon fibre revestment was increased to finally a rotor of pure carbon fibre. The best result was achieved with pure carbon fibre. Source: [10].

2. Materials and Methods

The authors have experience with instrumentation [12–14], which aided in the development of this work. A variety of flywheels were simulated by finite element modelling using SOLIDWORKS [15] with geometries studied by Coppede and Nogueira [11,16]. The adopted FEM simulation characteristics are shown in Table 2. The characteristics of carbon fibre Hexcel UHM 12000 appear in reference [10]; there are new carbon fibres with more resistance but the resistance was kept the same to allow comparison.

Some of the authors have experience with detection of gravitational waves [17], with many works using SOLIDWORKS [18–21].

Table 2. Finite Elements characteristics.

Type-of-Analysis	static analysis
Type-of-Meshing	solid
Thermal-effect	activated
Load-type	centrifugal
Connector-Support-type	bearing

3. Results

3.1. First Analysed Models

The simulations presented below are characterised as solid cylindrical bodies. All geometries are generally cylindrical with 200 mm of external diameter and about 100 mm of height. The results of the simulations are shown in Figure 3 and Table 3.

Preprints (www.preprints.org) | NOT PEER-REVIEWED | Posted: 12 December 2023 doi:10.20944/preprints202312.0530.v1

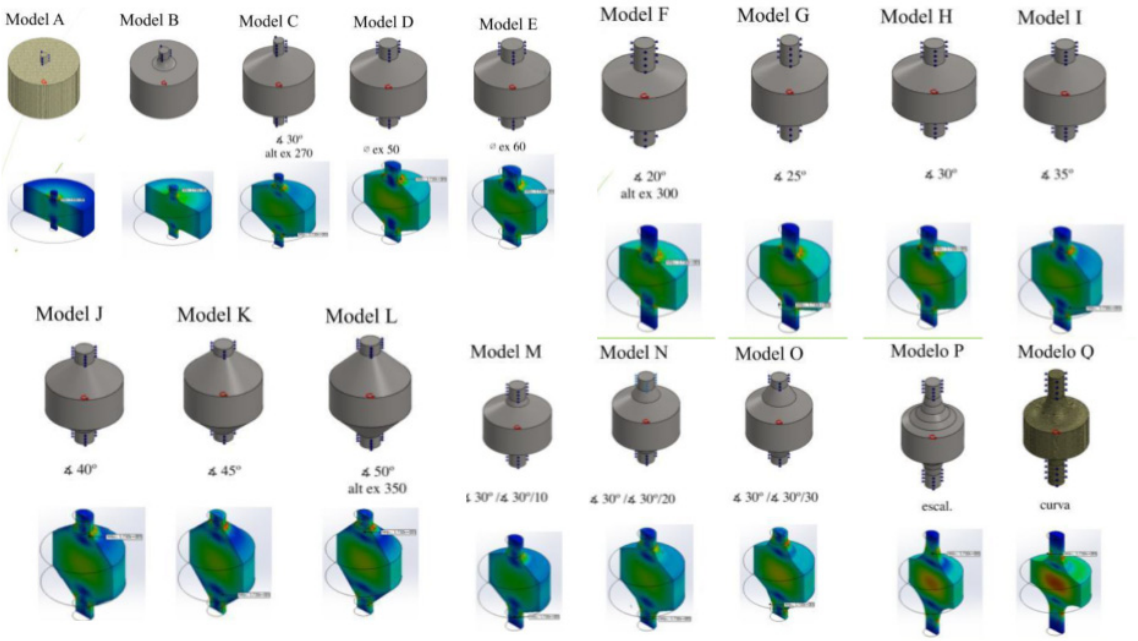

Figure 3. Models are labelled from A to Q. The bearings are located in the very top and in the very bottom of the flywheels. Source: The authors.

As the Q model presented a better behaviour and there was an indication that to increase the energy density the model needed to present a more uniform distribution in tensile stress, then a model with 180 mm of external diameter and 130 mm of height was developed, with a shape defined by the revolution of a Gaussian curve, justified next.

Following the sequence of the changes in the geometry, it is known that the best outcome results from the geometry that makes the stress get more homogeneous in the rotor. It seems quite reasonable that the best result will be reached if the whole section of the rotor experiences maximum stress. A calculation was made and the shape that allows this condition is a Gaussian shape, with formula

$$t = to\, e^{-\frac{\rho\omega^2 r^2}{2\sigma}} \quad (2)$$

where ϱ is the mass density, ω is the rotational velocity and σ is the resistance stress.

This Gaussian parameter was the one defined by Stodola [22], which is the formulation for a disk with constant stress, where the exponential squared parameter is the ratio of the squared rotational speed times specific mass divided by 2 times the ultimate tensile stress. This model is denominated **R**, where the central shaft with 20 mm diameter extends a further 20 mm on each side of the flywheel (see Figure 3). In Table 3 the results of all simulations can be found. The new model **R** (Figure 3) shows for highest rotation and energy density the best results, as the total energy and mass depend on the size of the flywheel.

Preprints (www.preprints.org) | NOT PEER-REVIEWED | Posted: 12 December 2023 doi:10.20944/preprints202312.0530.v1

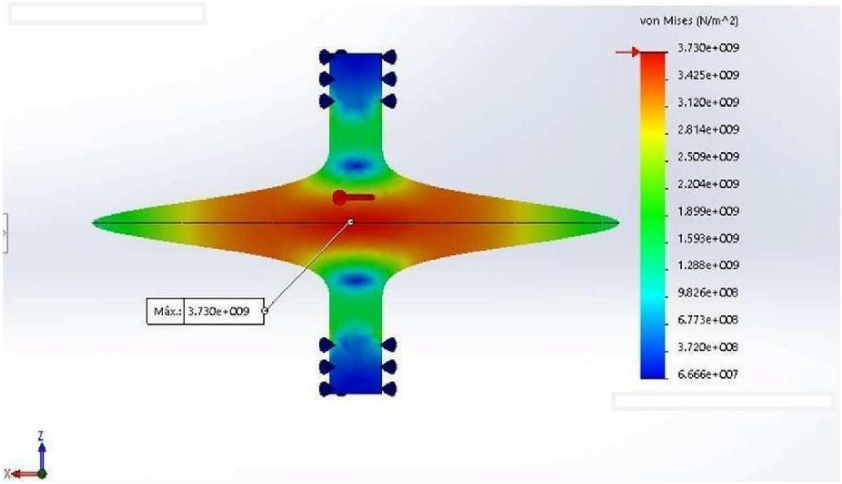

Figure 3. Von Mises stress for the R model. Source: the authors.

Table 3. Results of the simulations for different flywheel models. The best results are bolded.

Model	Maximum rotation speed (RPM)	Mass (kg)	Stored energy (Wh)	Energy density (Wh/kg)
A	162000	5.89	1176	199
B	153000	6.02	1053	175
C	167000	8.23	1528	185
D	192000	8.4	2042	243
E	185000	8.54	1905	223
F	187000	7.81	1803	231
G	192000	8.15	1964	241
H	194000	8.51	2086	245
I	185000	8.92	1967	220
J	186000	9.38	2065	220
K	182000	9.91	2080	210
L	188000	**10.73**	**2328**	217
M	163000	8.54	1468	172
N	176000	8.64	1715	199
O	189900	8.82	2013	228
P	195440	9.33	2145	230
Q	204820	8.16	2081	255
R	**279180**	0.96	374	**387**

3.2. Adding Mass to the Rotor Edge

The next step to increase the energy density in the rotor was to add some mass to the rotor. As can be seen in Figure 3, the von Mises stress at the edge of the rotor is lower because there is little mass on the very edge to create significant centrifugal force. Therefore, adding mass to the extremities is expected to generate more force. In Figure 3 the new design is presented, with mass added to the rotor's edge and the masses having a diamond cross section; the model will be called after the dimensions of this diamond cross section. Table 4 shows the results.

Preprints (www.preprints.org) | NOT PEER-REVIEWED | Posted: 12 December 2023 doi:10.20944/preprints202312.0530.v1

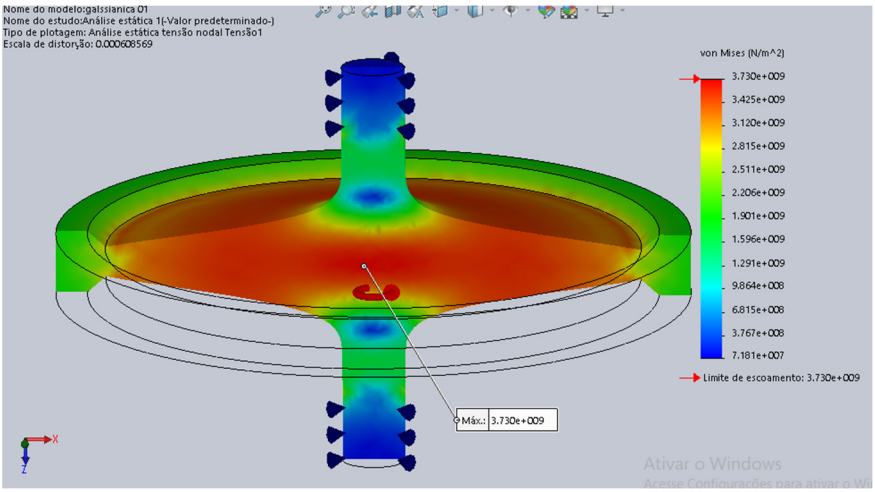

Figure 4. Von Mises stresses for the R model with mass added to the edge of the rotor. Source: the authors.

Table 4. Results of flywheel simulations with mass added to the rotors' edges. The second column shows the maximum rotational speed in rpm.

	RPM max	Mass (kg)	Energy (kJ)	Energy Density (kJ/kg)
Model Q	205,000	8.161	7491	918
Model R	279,000	0.968	1,347	1,392
Diamond 15x05	265,000	1.058	1,532	1,448
Diamond 15x10	259,000	1.109	1,601	1,451
Diamond 15x15	255,000	1.136	1,635	1,439
Diamond 20x05	259,000	1.098	1,603	1,459
Diamond 20x10	250,000	1.174	1,704	1,452
Diamond 20x15	240,000	1.238	1,238	1,382
Diamond 30x05	250,000	1.179	1,746	1,482
Diamond 30x10	227,000	1.315	1,754	1,335
Diamond 30x15	222,000	1.296	1,656	1,278

3.3. Double and Triple Flywheel Rotors

As the masses of these rotors are small, the total energy stored in a flywheel is equally small. In order to increase the total energy stored in each flywheel the model was modified to include two or three rotors with a Gaussian shape. In Figure 5 a flywheel is shown with a double Gaussian rotor and in Figure 6 there is an example of a flywheel with a triple gaussian rotor. In Table 5 there is an example of total energy, total mass, maximum rotation and energy density for a triple gaussian rotor.

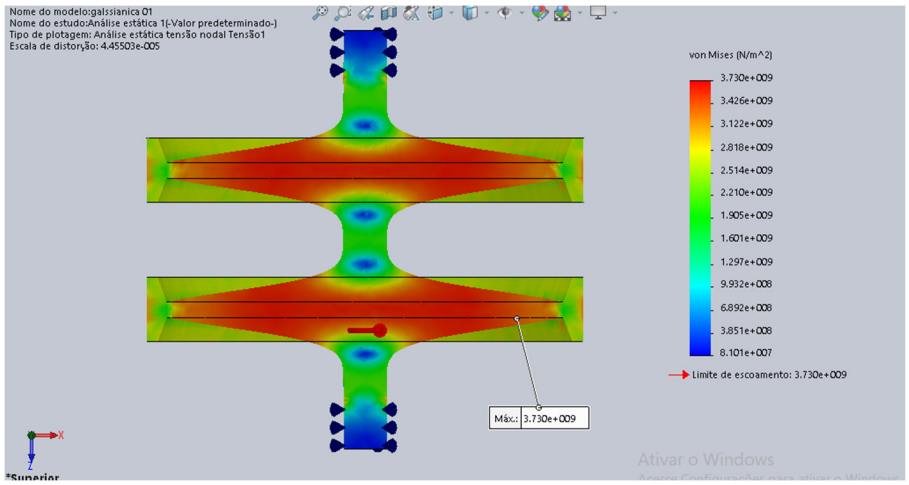

Preprints (www.preprints.org) | NOT PEER-REVIEWED | Posted: 12 December 2023 doi:10.20944/preprints202312.0530.v1

Figure 5. Double rotor flywheel example. Source: the authors.

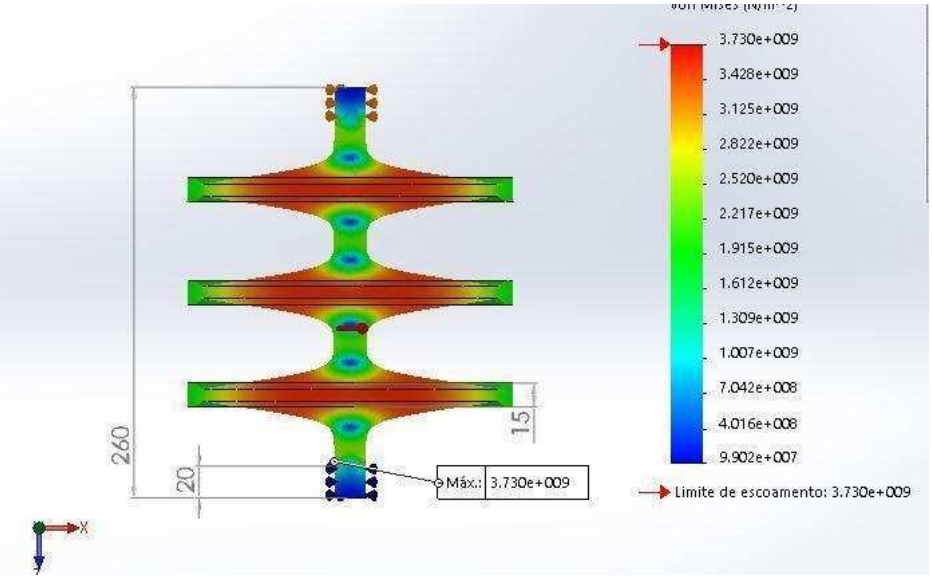

Figure 6. Triple rotor flywheel example Source: the authors.

Table 5. Maximum rotation, total mass, total energy and energy density for a triple rotor.

	Max. rotation (rpm)	Mass (kg)	Energy (J)	Energy density (J/kg)
diamond 15x05 Triple	268080	3.08	4777717	1549471

3.4. Vibrational Modes for Stability

One of the main concerns when working at very high rotational speeds is the stability of the rotor. As the rotor spins, small variations in its shape create torques that could excite the rotor normal modes of vibration that, under resonance, could destroy the rotor and the flywheel.

In order to avoid such a situation, the vibrational normal modes of the flywheels were simulated to have their frequencies found. An example is shown in Figure 7,whose first normal mode has a frequency of 0.086 Hz and is characterised by the masses added to the edges of the Gaussian rotor vibrating up and down in the system's axial direction. This mode is very inconvenient, as all the harmonics of this frequency could resonate with the rotation torque. These masses at the edges do not help much in increasing the energy density, so the best option seems to be to withdraw them from the flywheel. Therefore, all flywheel rotors now are formed only by the Gaussian-shaped ring. A double rotor vibration mode can be seen in Figure 8 with only Gaussian disks and showing no signal of vibration as this model presents a frequency of zero for this mode with no amplitude of vibration.

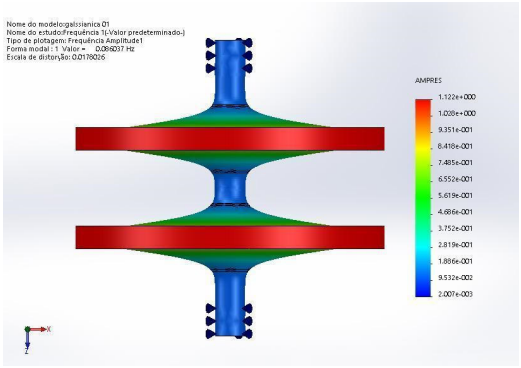

Figure 7. First vibration mode of a double rotor. Source: the authors.

Preprints (www.preprints.org) | NOT PEER-REVIEWED | Posted: 12 December 2023 doi:10.20944/preprints202312.0530.v1

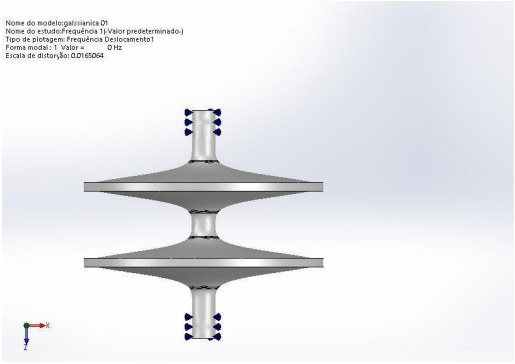

Figure 8. Double rotor with only Gaussian disks, zero frequency of vibration and no vibration amplitudes. Source: the authors.

The normal modes were then found with the simulations for the double and triple flywheel rotors. The respective frequencies and their harmonics could be avoided by the flywheel control system of the electromechanical battery; this job is reasonable as there are few of these modes in the flywheel operational range, Figure 9 and Figure 10 show these results. For the double rotor the first normal mode appears at a frequency of 1151 Hz, for a single rotor this frequency appears at 3341 Hz, these are the normal modes that appear in the operational range up to 4000 Hz in both cases.

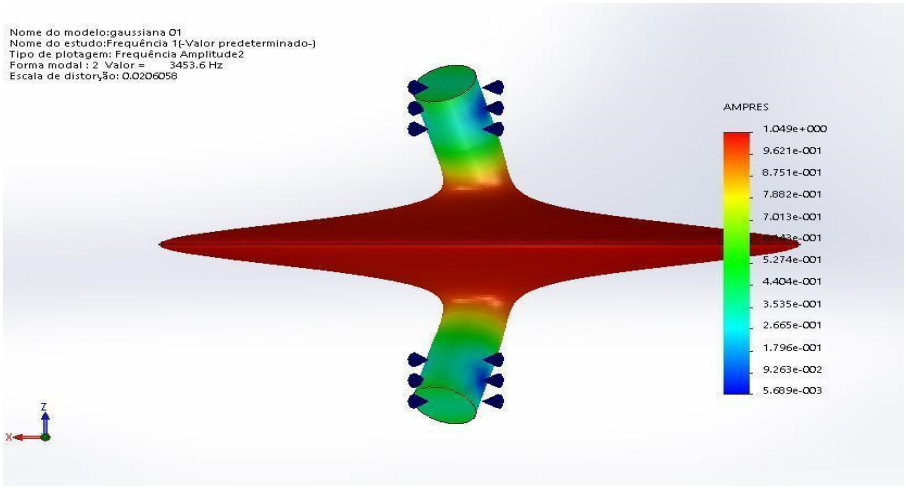

Figure 9. Single rotor first and only normal mode in the operational range up to 4000 Hz at a frequency of 3453 Hz. Source: the authors.

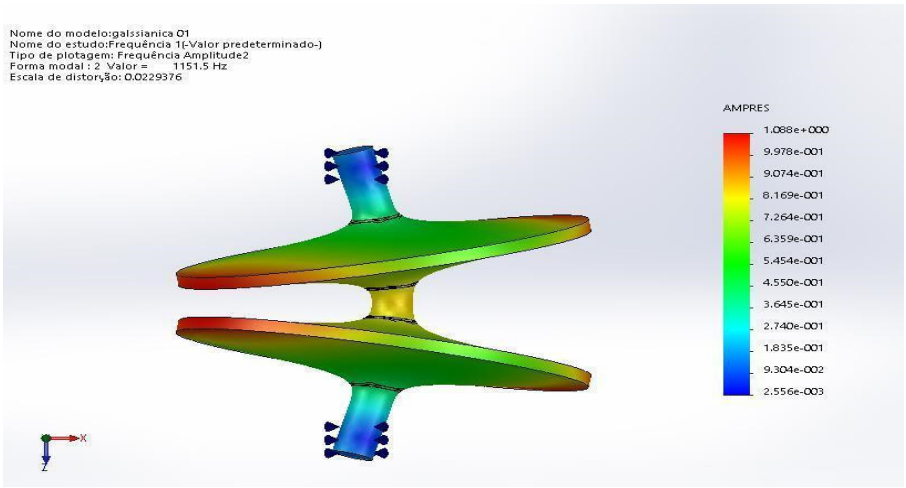

Preprints (www.preprints.org) | NOT PEER-REVIEWED | Posted: 12 December 2023 doi:10.20944/preprints202312.0530.v1

Figure 10. Double rotor first and only normal mode in the operational range up to 4000 Hz at a frequency of 1151 Hz. Harmonics must be considered. Source: the authors.

In order to avoid the instability of the double rotor flywheel a reinforcement was added connecting both disks, as shown in Figure 11. The frequency of the first normal mode first was calculated as 2500 Hz. It can be changed to a higher value by making the bearing axes shorter. This was not done in the simulation as this length is necessary for the simulation to run. There is also the possibility of improvement making the reinforcement wider. Figure 12 shows the simulation of this reinforced double rotor and presents an energy density of 403 Wh/kg or 1.45 MJ/kg, with some room for improvements as the point of maximum von Mises stress stress is located on the surface of the gaussian curve of the shaft.

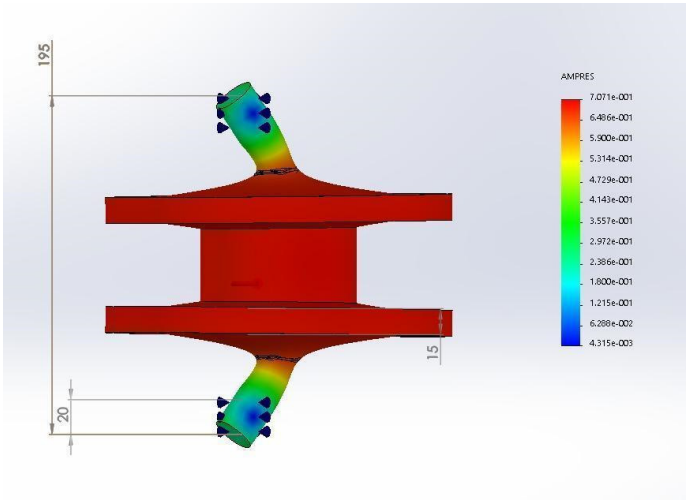

Figure 11. First and only normal mode up the operational frequency of the reinforced flywheel double rotor at the frequency of 2500 Hz. Source: the authors.

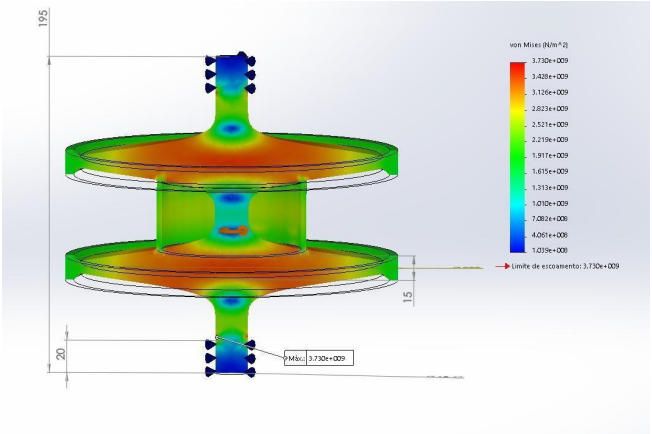

Figure 12. Simulation of von Mises stress in the reinforced double rotor flywheel. Source: the authors.

Figure 13 shows the same simulation for the reinforced triple rotor, which presents the same energy density of 403 Wh/kg or 1.45 MJ/kg, with some room for improvements as the point of maximum von Mises stress is located on the surface of the support axis.

Preprints (www.preprints.org) | NOT PEER-REVIEWED | Posted: 12 December 2023 doi:10.20944/preprints202312.0530.v1

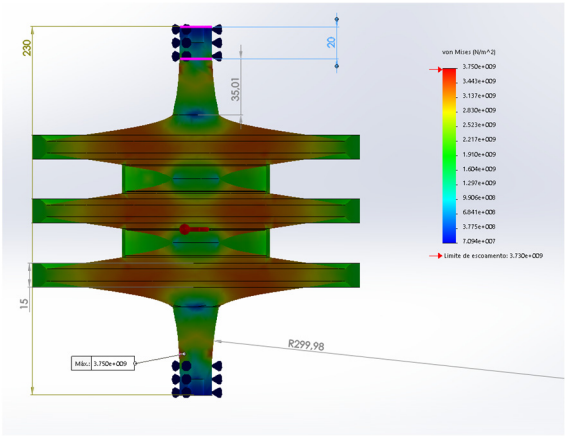

Figure 13. Simulation of von Mises stress in the reinforced triple rotor flywheel. Source: the authors.

4. Discussion

This work shows a case study of many flywheel rotors' geometries by the use of FEM simulations. All flywheel rotors were assumed to be made of carbon fibre Hexcel UHM 12000. Eighteen different geometries were analysed, comparing: maximum rotational speed, total stored energy, total mass and specific stored energy. An analysis of the von Mises stress was made in all models, showing the critical stress points.

In regard to the total stored rotational energy, Model **L** presented the highest value of 2328 Wh. However, as it has a relatively large mass of 10.731 kg the respective energy density is only 216.97 Wh/kg, which is lower than most of the other models.

The model **R,** with the Gaussian-shaped rotor, presents the highest value for the specific energy, with a value of 387 Wh/kg, and the largest rotational speed of 279180 rpm.

As for the triple rotor, it reached an energy density of 431 Wh/kg, which is about 56% higher than the one found using eqn. (1) for the same Hexcel UHM 12000 carbon fibre (≈277 Wh/kg). There are more resistant carbon fibres available in the market, but this work kept it constant to allow for comparisons.

There is more room for improvement, but not much as almost all the volume of the flywheel is filled with high von Mises stress.

Possible instabilities due to normal rotational modes were found at the operational frequency, being one mode for each kind of flywheel rotor. These frequencies must be avoided at all costs in the flywheel's operation, a process that can be easily implemented by a flywheel control system that can accelerate or decelerate the device as passing by these frequencies redirecting energy from one device to another as these devices operate in pairs.

The double and triple rotors can have their instability issues reduced by the use of a reinforcement tube connecting the two Gaussian disks that does not degrade the specific rotational energy much. As an example, we found that the reinforced double rotor has an energy density of 403 Wh/kg, also allowing room for improvement. This improvement will reach a maximum of 100%, where all the volume of the Flywheel has the maximum stress allowed in the material.

The results of this work are references for future investigations on the next steps for manufacturing an actual flywheel especially if they are made of carbon nanotubes, which are very expensive materials. If materials has enough resistance the storage density energy can reach the same values of common liquid fuels.

In the case carbon nanotubes can not be used because they could not be fabricated in long enough dimensions, the natural way is to use carbon fibres, as their resistance is improving with time.

The next step of this work is to simulate the resistance of these Flywheel rotors made of laminated carbon fibres aligned in the radial direction, the direction were the efforts are higher.

Author Contributions: Conceptualization: Carlso Frajuca; methodology: Carlos Frajuca and Fabio da Silva Bortoli; software: Daniel Coppede; validation: Carlos Frajuca and Daniel Coppede; formal analysis: all the

authors; investigation: all the authors.; resources: Daniel Coppede; writing—original draft preparation: Carlos Frajuca and Nadja Simao Magalhaes; writing—review and editing: Nadja Simao Magalhaes; supervision: Carlos Frajuca and Fabio da Silva Bortoli; project administration: Carlos Frajuca and Joao Manoel Lozada Moreira; funding acquisition, Carlos Frajuca, Fabio da Silva Bortoli and Daniel Coppede

Funding: This research was funded by FAPESP through grant #2013/26258-4 and by CNPq through grant #312454/2021-0. The APC was funded by vouchers.

Conflicts of Interest: The authors declare no conflict of interest.

References

1. Junling, C.; Xinjian, J.; Dongqi, Z.; Haigang, W. A Novel Uninterruptible Power Supply using Flywheel Energy Storage Unit. In Proceedings of The 4th International Power Electronics and Motion Control Conference - IPEMC 3, 2004, pp. 1180.
2. Stephan, R.M.; Andrade, Jr.R.; Sotelo, G.G. Third Generation of Flywheels: a Promising Substitute to Batteries. *Revista Eletronica de Potencia* **2008,** 13, pp. 171.
3. Fiske, O.J.; Ricci, M.R. Third Generation Flywheels For High Power Electricity Storage. *LaunchPoint Technologies*, Inc., 2016 Goleta, California, USA. Available online: https://www.launchpnt.com/hs-fs/hub/53140/file-14467597-pdf/docs/002_fiske_powerring.pdf.
4. Bankston, S.; Mo, C. Geometry Modification of Flywheels and its Effect on Energy Storage. *Energy Res. J.* **2015**, 6, 54.
5. IRENA. International Renewable Energy Agency. Electricity Storage and Renewables: Costs and Markets to 2030. *International Renewable Energy Agency*, **2017** Abu Dhabi.
6. Ribeiro, M.R. Sistema Armazenador de Energia Cinetica SAEC - Estrategia de Controle e Simulacoes. Rio de Janeiro: MSc thesis - COPPE/UFRJ, Brazil, 2008.
7. Hedlund, M.; Lundin, J.; de Santiago, J.; Abrahamsson, J.; Bernhoff, H. Flywheel Energy Storage for Automotive Applications. *Energies* **2015**, 8, 10636.
8. Ashby, M.F. 2017 *Materials Selection in Mechanical Design*. Fifth edition, Elsevier Ltd., Cambridge, United States.
9. Wang, B. CNT bundle material for flywheels: 40 times better than batteries. 2018. Available https://www.nextbigfuture.com/2018/10/cnt-bundle-material-for-flywheels-40-times-better-thanbatteries.html.
10. MatWeb - The Online Materials Information Resource. Available online: http://www.matweb.com
11. Coppede, D. Análise por Simulação de Materiais Conjugados para Baterias Eletromecânicas. MSc thesis - IFSP, Sao Paulo, Brazil, 2018.
12. Bortoli, F.S.; Frajuca, C.; Sousa, S.T.; de Waard, A.; Magalhaes, N.S.; Aguiar, O.D. On the massive antenna suspension system in the brazilian gravitational wave detector Schenberg. *Braz. J. Phys.* **2016,** 46, 308.
13. Andrade, L.; Costa, C. Aguiar, O.D.; Frajuca, C.; Mosso, M.; Podcameni, A.; Da Silva, H.; Magalhaes, N.S. Ultra-low phase noise 10 Ghz oscillator to pump the parametric transducers of the mario Schenberg gravitational wave detector. *Class Quantum Gravity* **2004**, 21, S1215.
14. Bortoli, F.S.; Frajuca, C.; Magalhaes, N.S.; Duarte, E.N. A physical criterion for validating the method used to design mechanical impedance matchers for mario schenberg's transducers. *J. Phys. Conf. Ser.* **2010,** 228, 012001.
15. SOLIDWORKS. Available online: https://www.solidworks.com.
16. Nogueira, P.R.M. Otimizacao de Geometria e Material para Baterias Eletromecanicas. MSc thesis - IFSP, Sao Paulo, Brazil, 2016.
17. Aguiar, O.D.; et al. The gravitational wave detector "Mario Schenberg": Status of the project. *Braz. J. Phys.* **2002**, 32, 866.
18. Frajuca, C.; Bortoli, F.S.; Magalhaes, N.S. Resonant transducers for spherical gravitational wave detectors. *Braz. J. Phys.* **2005**, 35, 1201.
19. Frajuca, C.; Bortoli, F.S.; Magalhaes, N.S. Studying a new shape for mechanical impedance matchers in Mario Schenberg transducers. 2006 *J. Phys. Conf. Ser.* **2006,** 32, 319.
20. Frajuca, C.; Souza, M.A.; Coppede, D.; Nogueira, P.R.M.; Bortoli, F.S.; Santos, G.A.; Nakamoto, F.Y. *J. Braz. Soc. Mech. Sci. Eng.* **2018**, 40, 319.
21. Bortoli, F.S.; Frajuca, C.; Magalhaes, N.S.; Aguiar, O.D.; Souza, S.T. On the cabling seismic isolation for the microwave transducers of the Schenberg detector. 2019 *Braz. J. Phys.* **2019**, 49, 133.
22. Kress, R. Shape optimization of a flywheel. *Struc. Multidiscipl Optim* **2000**, 19, 74.